Energy Funneling in a Non-Integer Two-Dimensional Perovskite

Alexander M. Oddo,[1,3,†] Mengyu Gao,[2,3,†] Daniel Weinberg,[1,3] Jianbo Jin,[1] Maria C. Folgueras,[2,3,4] Chengyu Song,[5] Colin Ophus,[5] Tomoyasu Mani,[6] Eran Rabani,[1,3,7] and Peidong Yang[1,2,3,4,]*

1 Department of Chemistry, University of California, Berkeley, Berkeley, California 94720, United States

2 Department of Materials Science and Engineering, University of California, Berkeley, Berkeley, California 94720, United States

3 Materials Sciences Division, Lawrence Berkeley National Laboratory, Berkeley, California 94720, United States

4 Kavli Energy NanoScience Institute, Berkeley, California 94720, United States

5 National Center for Electron Microscopy, Molecular Foundry, Lawrence Berkeley National Laboratory, Berkeley, California 94720, United States

6 Department of Chemistry, University of Connecticut, Storrs, Connecticut 06269-3060, United States

7 The Raymond and Beverly Sackler Center of Computational Molecular and Materials Science,

Tel Aviv University, Tel Aviv 69978, Israel

Abstract

Energy funneling is a phenomenon that has been exploited in optoelectronic devices based on low-dimensional materials to improve their performance. Here, we introduce a new class of two-dimensional semiconductor, characterized by multiple regions of varying thickness in a single confined nanostructure with homogenous composition. This "non-integer 2D semiconductor" was prepared via the structural transformation of two-octahedron-layer-thick (*n=2*) 2D cesium lead bromide perovskite nanosheets; it consisted of a central *n=2* region surrounded by edge-lying *n=3* regions, as imaged by electron microscopy. Thicker non-integer 2D $CsPbBr_3$ nanostructures were obtained as well. These non-integer 2D perovskites formed a laterally coupled quantum well band alignment with virtually no strain at the interface and no dielectric barrier, across which unprecedented intramaterial funneling of the photoexcitation energy was observed from the thin to the thick regions using time-resolved absorption and PL spectroscopies.

Perovskite, heterostructure, nanocrystal, photophysics, TEM

It is essential to build a fundamental view connecting the structure of semiconductors to their photophysical properties, which ultimately determines the performance of optoelectronic devices. Metal halide perovskites stand out because they tout numerous attractive features for optoelectronic applications, such as high absorption coefficients, easily tunable bandgaps, relative defect tolerance, and long carrier diffusion lengths[1-3]. Following a decade of research, the photoluminescence quantum yield (PLQY) of lead halide perovskite quantum dots has reached unity[4], the efficiency of perovskite-based solar cells currently exceeds 33%[5], and perovskite-based photodetectors are competitive against those made from silicon[6].

Two-dimensional (2D) metal halide perovskites are of specific interest because they outcompete their bulk counterparts in terms of optical performance and environmental stability[7-9], which is among the most pervasive issues limiting the proliferation of perovskite materials into mainstream applications. However, the primary challenge with 2D perovskite is that confinement precludes the formation of long-lived free carriers through competition with strongly bound, radiative excitons[7-10]. This ultimatum in confined semiconductors has motivated the exploration of perovskite dimensionality to achieve a material with optimal optoelectronic performance and stability. The strategy of energy funneling has been developed to treat the adverse effects of confinement[10-15]. The bandgap of 2D perovskite scales with material thickness due to confinement[10-15]. In energy funneling, the photoexcitation energy is funneled downhill along a bandgap gradient formed by a distribution of packed 2D perovskites that increase in thickness, known as quasi-2D perovskites[10-15]. The goal of energy funneling is to accumulate excited species on the thickest 2D perovskite, which is idealized by lower exciton binding energy[1,10-15]. From the thickest 2D perovskite, the enhanced emission rate can then be exploited for light-emitting diode or lasing applications, or charge may be extracted more readily for solar cells[10-15].

However, a fraction of the photoexcitation energy is lost with each successive transfer event in energy funneling depending on the dielectric constant of the ligand spacers surrounding the perovskite lattice[15-19]. Such efficiency loss has motivated further research on energy transfer[1,19-22], ligand shell chemistry[23,24], and the development of alternative approaches to improve energy funneling. Such includes superlattices with strong electronic coupling[25-28], compositional core/shell, core/crown, and ionic heterostructures[29-36], Van der Waals heterostructures[37,38], mixed dimensionality nanostructures[39,40], and dielectric doping[41-43].

In this regard, we propose a novel material characterized by thickness heterogeneity within a single 2D nanostructure, which we term a "non-integer 2D semiconductor." The absence of ligands between regions of different perovskite thicknesses in the non-integer system forms a downhill band alignment without dielectric barriers, which may circumvent the obstacles faced by quasi-2D perovskites in energy funneling. We report the occurrence of intramaterial energy funneling from thinner to thicker regions, evidenced by time-resolved photoluminescence (PL) and femtosecond transient absorption (fsTA) spectroscopies. Based on atomic resolution transmission electron microscopy (TEM) imaging and structural modeling, the interface across which transfer took place was virtually strain-free, unlike that present in heterostructures of varying elemental composition. Furthermore, this work unveils confinement as a knob to tune the interfaces and properties of semiconductors local to a single nanoparticle and highlights the implications of thickness variability on the optoelectronic properties of semiconductors, portending immediate device applications.

It has been established that perovskites are amenable to post-synthetic modification due to their soft, ionic lattice. For instance, bandgap tunability in perovskites has been achieved via anion exchange[1], and their morphology can even change in the presence of polar solvent[44]. In this

work, non-integer 2D perovskites were formed by the introduction of polar ligands to colloidal cesium lead bromide nanosheets (Figure 1a), leveraging the dynamic ligand environment and lability of perovskite to induce desirable structural transformation. The product of this reaction was a previously undiscovered 2D nanostructure resembling the parent nanosheet, but with thickened edges. 2D perovskites are identified by their thickness (phase number) in units of octahedra, $n=x$. Therefore, we term the nonuniform-thickness products of the structural transformation reaction, "non-integer," because they cannot be fully described by just one integer phase number.

The starting, colloidal nanosheets had an edge length around 100 nm (Figure 1b and S1). The cubic, two lead bromide octahedral layer-thick ($n=2$) $CsPbBr_3$ nanosheet was synthesized via our reported synthetic procedure with modifications[25]. The 2D morphology enabled the observation of intense, room-temperature excitons, with an absorption peak at 428 nm and a PL emission peak at 436 nm (Figure S2), both consistent with literature results on the assignment of $n=2$ $CsPbBr_3$ nanosheet thickness[25,45]. The cubic phase was confirmed with TEM (Figure S3). The $n=2$ nanosheets were also monodisperse in thickness, indicated by a single excitonic peak in the absorption and PL spectra. This high purity meant that optical measurements could be performed to unambiguously track the transformation of $n=2$ nanosheets into non-integer products containing different thicknesses of lead bromide octahedra, with different excitonic energies, alongside TEM for structural identification, as follows.

Aliquots of the reaction mixture were removed and purified throughout the reaction, which allowed for the study of non-integer products *ex situ* without further structural transformation. TEM imaging showed an increase in contrast growing at the edges of the nanosheets as the reaction progressed (Figure 1b–d). We note now that the nanosheet-loaded TEM grids were

encapsulated with graphene to avoid electron beam damage (Figure S4 and S5), as ultrathin $CsPbBr_3$ perovskite is notoriously beam-sensitive[46,47]. The integrated TEM image line scan intensity increased discretely at the edges of the non-integer structures (Figure 1e–g). Accompanying spikes in the derivative were consistent across the different non-integer 2D $CsPbBr_3$ phase compositions. This contrast change corresponded to the formation of a thicker $CsPbBr_3$ phase relative to the starting *n=2* phase. To identify the phase of the thickened edges of the nanosheet, we turned to absorption and PL spectroscopy.

In coincidence with TEM, an absorption study was conducted that tracked the transformation of the pure *n=2* excitonic absorption peak at 428 nm into another excitonic absorption peak at 454 nm (Figure 1h–j). The respective PL peaks were located at 436 nm and 463 nm. This exciton was lower in energy because quantum confinement was alleviated as the *n=2* nanosheets grew thicker. The absorption intensities coincided with the observed edge-thickening, as the *n=2* exciton diminished with the appearance of the 454 nm exciton. Furthermore, the appearance of another exciton at a different wavelength, rather than continuous redshift, implied that the non-integer nanostructure was formed with discrete thickness resolution. This resolution was that of a single lead bromide octahedron layer, as the 454 nm exciton (463 nm PL) matched that of pure, as-synthesized *n=3* $CsPbBr_3$ nanosheets (Figure S6). Thus, we assign the growing, higher contrast edges of non-integer 2D $CsPbBr_3$ to the *n=3* phase and the lower contrast interior to the starting *n=2* phase, both present in a single nanostructure. To the authors' knowledge, this is the first report of such a non-integer 2D semiconductor. While the *n=2:3* non-integer $CsPbBr_3$ perovskite is the model system of focus in the main text, further reaction yielded similarly interesting *n=3:4* $CsPbBr_3$ in the form of nanoframes and abnormal, sawtooth nanostructures. A

collection of TEM images of all non-integer 2D $CsPbBr_3$ along with discussion of the structural transformation reaction can be found in the Supporting Information (Figure S7–S11).

We now aim to substantiate our claim that this non-integer concept is an alternative approach to accomplish energy funneling. We hypothesize that the attached *n=2* and *n=3* phases of the non-integer perovskite forms double quantum well with in-plane type-I alignment (Figure 2a). This contrasts with quasi-2D perovskites in which the ligand barrier interrupts the type-I alignment (Figure 2b)[14-19,48,49]. Above bandgap photoexcitation produced the expected PL spectrum of the *n=2:3* 2D perovskite, which consisted of exciton emission from the *n=2* and *n=3* phases as seen in the 2D photoluminescence-excitation spectrum (PLE, Figure 2c). However, direct photoexcitation of the *n=2* exciton compared to above bandgap photoexcitation caused greater intensity, or sensitized, emission from the *n=3* exciton, as evident by the excitation spectrum viewed at the 463 nm emission wavelength (Figure 2c, inset) and when compared to the *n=3* nanosheet control (Figure S12). Furthermore, excitation between the optical bandgaps of the *n=2* and *n=3* excitons did not produce strong emission, and even direct excitation of the *n=3* exciton at 454 nm produced relatively weak emission. Additionally, electronic structure calculations of a non-integer 2D perovskite showed that the highest occupied molecular orbitals of the *n=2* phase extended across the *n=2:3* interface (Figure S13). The PLE along with computations implied electronic coupling between the *n=2* and the *n=3* phases and supported the occurrence of energy funneling. The same was true for higher order non-integer 2D $CsPbBr_3$ (Figure S14).

The transfer of photoexcitation energy in a donor-acceptor system is more authentically represented by a change in photodynamics. The PL decay of the *n=2* and *n=3* excitons of the pure *n=2* and *n=3* $CsPbBr_3$ nanosheets was triexponential, with respective lifetimes of 16 and 30

ns representing the timescale trapping/detrapping process, accompanied by lifetimes <7 ns (Figure S15). The corresponding PL lifetimes of the *n=2* and *n=3* excitons in *n=2:3* $CsPbBr_3$ differed from those of the pure phases, and indicated PL quenching of the *n=2* exciton but not the *n=3* exciton. Two distinct regions were seen in the PL decay map of the 40% *n=3* $CsPbBr_3$ (Figure 2d), which corresponded to the *n=2* phase in the presence of the *n=3* phase and vice versa. The increase in PL lifetime from the *n=2* region to the *n=3* region was expected because of the alleviation of quantum confinement with increasing $CsPbBr_3$ thickness as well as the aforementioned quenching of the *n=2* exciton by the *n=3* phase. This quenching behavior was observed by measuring the PL decay as a function of phase composition in the *n=2:3* $CsPbBr_3$ (Figure 2e). The 16 ns PL lifetime of the *n=2* exciton in the pure *n=2* nanosheet was quenched by a factor of 2.2 in the 40% *n=3* $CsPbBr_3$, which was direct evidence of photodynamic transfer from the *n=2* phase to the *n=3* phase. The relative contribution of this PL lifetime to the PL decay decreased from 61.1% in the *n=2* nanosheet to 12.8% in the 40% *n=3* $CsPbBr_3$. In coincidence, the PLQY decreased from 31.9% for the pure *n=2* nanosheet to 22.5% for the 10% *n=3* $CsPbBr_3$ and to 10.4% for the 40% *n=3* $CsPbBr_3$. Concomitantly, the relative contribution of the shortest decay constant increased with increasing *n=3* phase composition. The intermediate PL lifetime, around ~2 ns, did not follow a trend as a function of phase composition. Based on the quenching of the PL lifetimes, high transfer efficiencies of 61% and 83% were calculated for the 10% *n=3* and the 40% *n=3* perovskites, respectively. Analogous lifetime mapping and PL lifetime results were obtained for the higher order non-integer 2D $CsPbBr_3$ (Figure S16–S21).

To gain further insight on the photodynamic transfer, we turned to femtosecond transient absorption spectroscopy (fsTA). Unless stated otherwise, all measurements were of solution-state

samples, which made it so interparticle transfer phenomena were diffusion-limited. The ground state bleach (GSB) of the pure *n=2* exciton was located around 428 nm (Figure 3a), matching that of the steady-state absorption, with decay constants of τ_1=216, τ_2=855, and τ_3=1197 ps. The τ_1 and τ_3 lifetimes of the GSB decay were consistent with the ~0.3 ns and ~2 ns radiative processes observed in the PL decay, respectively, while τ_2 corresponded to a nonradiative lifetime, as it did not contribute to the PL decay. The fsTA data of the pure *n=2* nanosheet served as a standard for comparison against that of the *n=2:3* perovskites. It was useful to deconvolute the dynamics by comparing to the pure *n=2* nanosheet as a control because both, the *n=2* and *n=3*, phases were excited above bandgap. The non-integer 2D perovskites measured via fsTA were of the phase compositions depicted in Figure 1c and 1d: 10% and 40% *n=3* (Figure 3b and 3c). The GSB of the *n=2* exciton was around 428 nm while that of the *n=3* exciton was around 454 nm, which matched the steady-state absorption. This can be seen more clearly in the corresponding fsTA spectral traces (Figure 3d and S22). There was further evidence that the photoexcitation energy was being funneled from the *n=2* phase to the *n=3* phase, as the radiative τ_1 and nonradiative τ_2 of the *n=2* exciton were quenched significantly with increasing *n=3* presence in the nanostructure (Figure 3e). Similarly, the excited state absorption at 410 nm was quenched with increasing *n=3* presence (Figure 3f). These conclusions were also true for the *n=3:4* $CsPbBr_3$ (Figure S23 and S24). The decay constants of all relevant GSB and excited state absorption (ESA) features can be found in Supporting Table 1. Furthermore, the rise of the *n=3* GSB was slower in the 40% *n=3* $CsPbBr_3$ than in the pure *n=3* nanosheet (Figure 3g). Kinetic modeling of the non-integer 2D perovskite successfully reproduced this behavior when a direct transfer channel was included between the conduction bands of the *n=2* and *n=3* phases (Figure 3h).

The mechanism by which the photoexcitation energy was transferred between the phases of the non-integer 2D perovskites will now be discussed. It is still a contended issue whether energy funneling in quasi-2D perovskites occurs by the energy or charge transfer mechanism and by what branching ratio[49]. Attempts to distinguish the two mechanisms in quasi-2D perovskite have been made using their characteristic timescales; hundreds of femtoseconds for energy transfer and tens of picoseconds for charge transfer. Most reports have sided with the exciton energy transfer mechanism[12-19,48], justified by a high degree spectral overlap and dipole alignment between the donor and acceptor in quasi-2D perovskite, meanwhile free carrier transfer is suppressed by the interparticle ligand barrier[48]. However, the ligand barrier is not present in non-integer 2D perovskite. We also measured the fsTA spectrum of a film containing a dropcasted mixture of pure *n=2* and *n=3* nanosheets (Figure 3e and S25). Since interparticle phenomena were no longer diffusion-limited in the solid-state, this film served as a control sample to mimic energy funneling in a quasi-2D perovskite made from just the *n=2* and *n=3* phases of $CsPbBr_3$. Fitting of the *n=2* exciton GSB decay in the solid sample returned decay constants of <0.01 ps, 0.600 ps, and 9.9 ps; the *n=2* exciton GSB of the pure nanosheet was quenched down to a factor of ~18,000. On the other hand, the dynamics observed for the non-integer 2D $CsPbBr_3$ occurred over hundreds of picoseconds. This suggested that charge transfer, which is characteristically slower than energy transfer, could be a mechanism of energy funneling or that energy transfer was uncharacteristically slow in *n=2:3* $CsPbBr_3$. To suit particular applications, we note that the funneling efficiency and kinetics can be modified according to the overlap between the donor emission and acceptor absorption, which depends on the elemental composition and the thickness of the 2D perovskite[48]. Ultimately, the disparity in the photodynamics between the

quasi-2D $CsPbBr_3$ imitation sample and non-integer 2D $CsPbBr_3$ affirms that the implication of structural heterogeneity in semiconductors is intramaterial energy funneling.

Photoexcitation transfer has been identified at interfaces of semiconductors with lateral band alignments, such as ionic heterojunctions and conventional heterostructures in composition, including core-shell and core/crown nanostructures[1,31-35]. However, ionic heterojunctions decompose via ion diffusion and lattice-mismatch strain at interfaces of conventional heterostructures can poison charge transfer and optical properties[1,29-36]. In conventional heterostructures, the charge transfer state is typically a trap state that arises from strain at the interface of the constituent semiconductors, which has motivated the search for interfaces with optimal lattice mismatch for device applications[1,32-36]. Further investigation of the *n=2:3* interface was warranted given that the strain behavior in this kind of heterostructure with constant elemental composition has not been explored before nor the consequences on energy funneling. Atomic resolution TEM was used to probe the *n=2:3* $CsPbBr_3$ lattice for a possible out-of-plane or in-plane structural interface. The pure *n=2* and *n=3* $CsPbBr_3$ nanosheets had a cubic lattice with a Pb-Br bond distance of 3.1 ± 0.1 Å, respectively (Figure S3 and S6). The *n=2:3* $CsPbBr_3$ also had a cubic lattice with a Pb-Br bond distance of 3.1 ± 0.1 Å. Therefore, a unique, out-of-plane structural interface was not discernable between the *n=2* and *n=3* phases (Figure 4a), confirming that *n=2* and *n=3* phases were attached coherently, with virtually no lattice strain between them. There were no Bragg peaks in the diffraction pattern (obtained by Fast Fourier Transform) of the *n=2:3* $CsPbBr_3$ compared to the pure *n=2* and *n=3* nanosheet controls that could indicate the distortion of Pb-Br bonds (Figure 4b–d) or the existence of the orthorhombic Cs_4PbBr_6 lattice[1]. This was true for both the global diffraction pattern of the non-integer 2D perovskite and that of the selected diffraction pattern local to the interface (Figure 4e). The

selected diffraction pattern of the *n=2:3* $CsPbBr_3$ was of a single cubic pattern, which confirmed that the growth of the third layer of octahedra on the *n=2* phase was perfectly epitaxial and disproved the existence of an in-plane interface. Structural modeling of the *n=2:3* $CsPbBr_3$ did not reveal an in-plane or out-of-plane interface either and showed that the crystal structure remained cubic throughout (Figure 4f). The implied *n=2:*3 interface across which energy funneling occurred was thus defined solely by confinement, which also makes this study among the first to demonstrate highly efficient transfer without the influence of strain in a heterostructure.

Energy funneling has been desired among 2D semiconductors to improve their performance in devices while maintaining the other advantageous properties gained from reduced dimensionality. While efforts so far have been focused on solving this problem using quasi-2D perovskite, we have successfully demonstrated that energy funneling can also occur in the $CsPbBr_3$-based non-integer 2D perovskite, which is the first of a new class of semiconductor. The structural transformation reaction demonstrated that a variety of non-integer 2D perovskites could be prepared with properties that depend on the non-integer character, such as the absorption and emission profile, PLQY, PL decay kinetics, and transfer efficiency. Unlike conventional heterostructures, the interface between phases of the non-integer 2D $CsPbBr_3$ was structurally coherent and virtually strain-free, which may permit the high transfer efficiencies desired for device applications. The overall findings presented herein necessitate further investigation and review of semiconductors with thickness heterogeneity in the confined regime and expansion of the non-integer concept to other materials and devices.

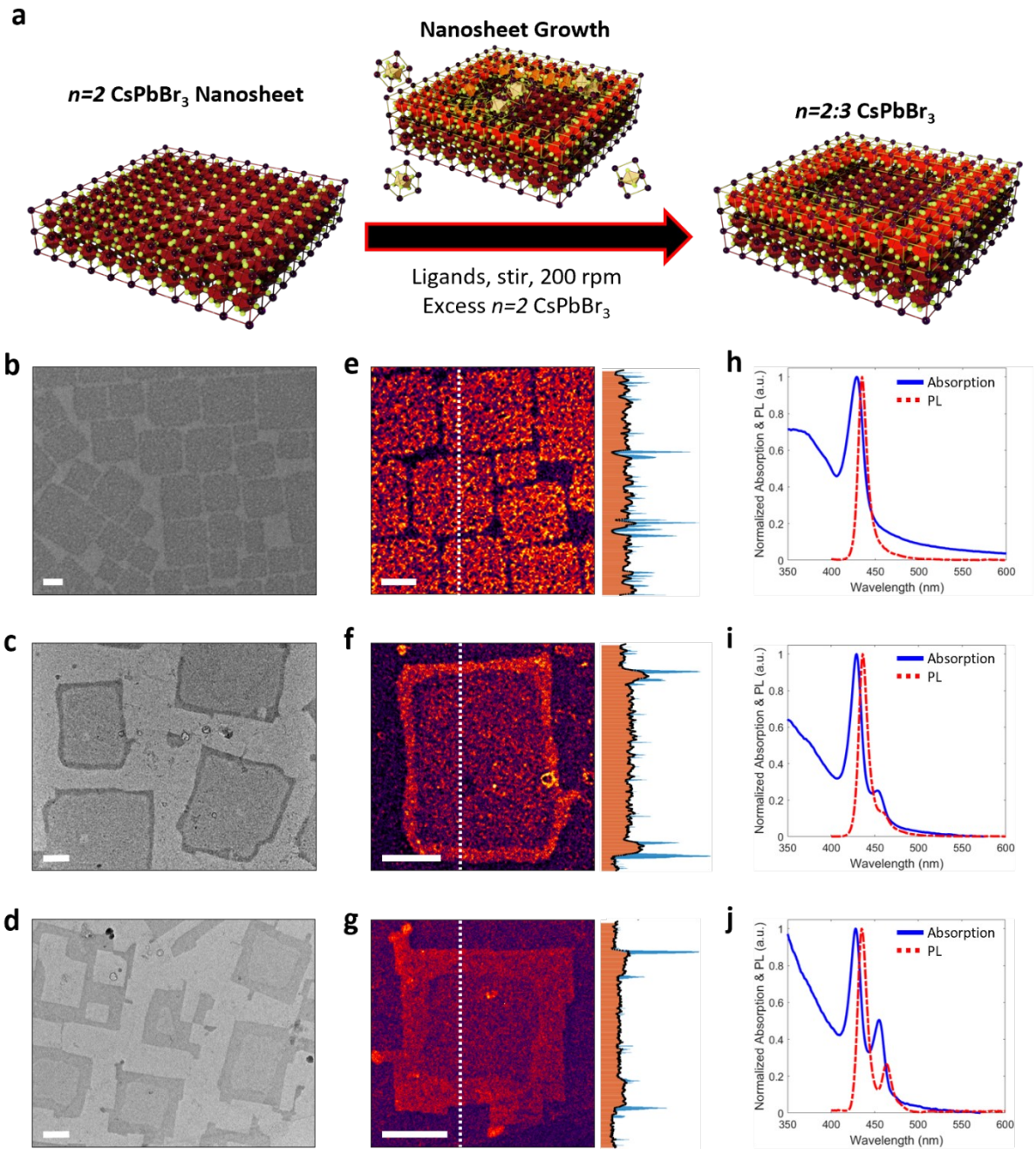

Figure 1. Characterization of *n=2:3* $CsPbBr_3$ growth. **a**, Schematic depicting the structural transformation of *n=2* $CsPbBr_3$ nanosheet to *n=2:3* $CsPbBr_3$ in the presence of ligands at room temperature. **b**, is the TEM image of *n=2* $CsPbBr_3$ nanosheets; **c**, and **d**, are that of *n=2:3* $CsPbBr_3$ containing 10% and 40% *n=3* composition, respectively. Scale bar: 50 nm. **e-g**,

Zoomed-in TEM images colored for high contrast and line scans containing the derivative of image intensity (blue). **h-j**, The corresponding absorption and PL spectra.

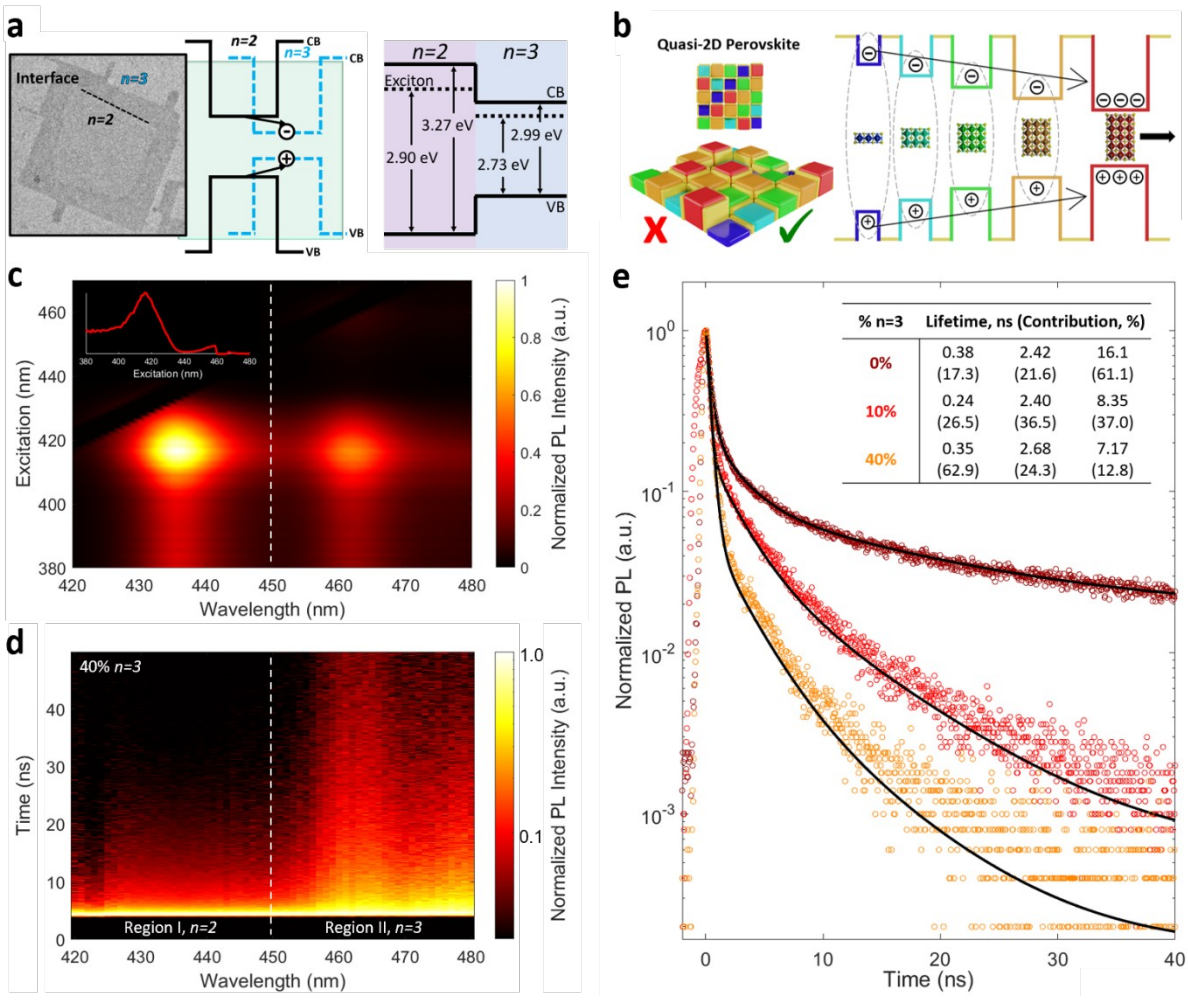

Figure 2. Photophysics of *n=2:3* $CsPbBr_3$ based on PL spectroscopy. **a**, Depiction of coupled quantum well structure of the *n=2:3* $CsPbBr_3$. **b**, Illustration of energy funneling in quasi-2D perovskite. **c**, 2D PLE spectrum of *n=2:3* $CsPbBr_3$ with 40% *n=3* composition. Inset: Normalized PL excitation spectrum viewed at the 463 nm emission wavelength. **d**, PL lifetime map of *n=2:3* $CsPbBr_3$ with 40% *n=3* composition. **e**, PL decay of *n=2* exciton at 436 nm with respect to the *n=3* composition. Inset: the corresponding PL decay constants and relative contributions in parenthesis (95% confidence fit).

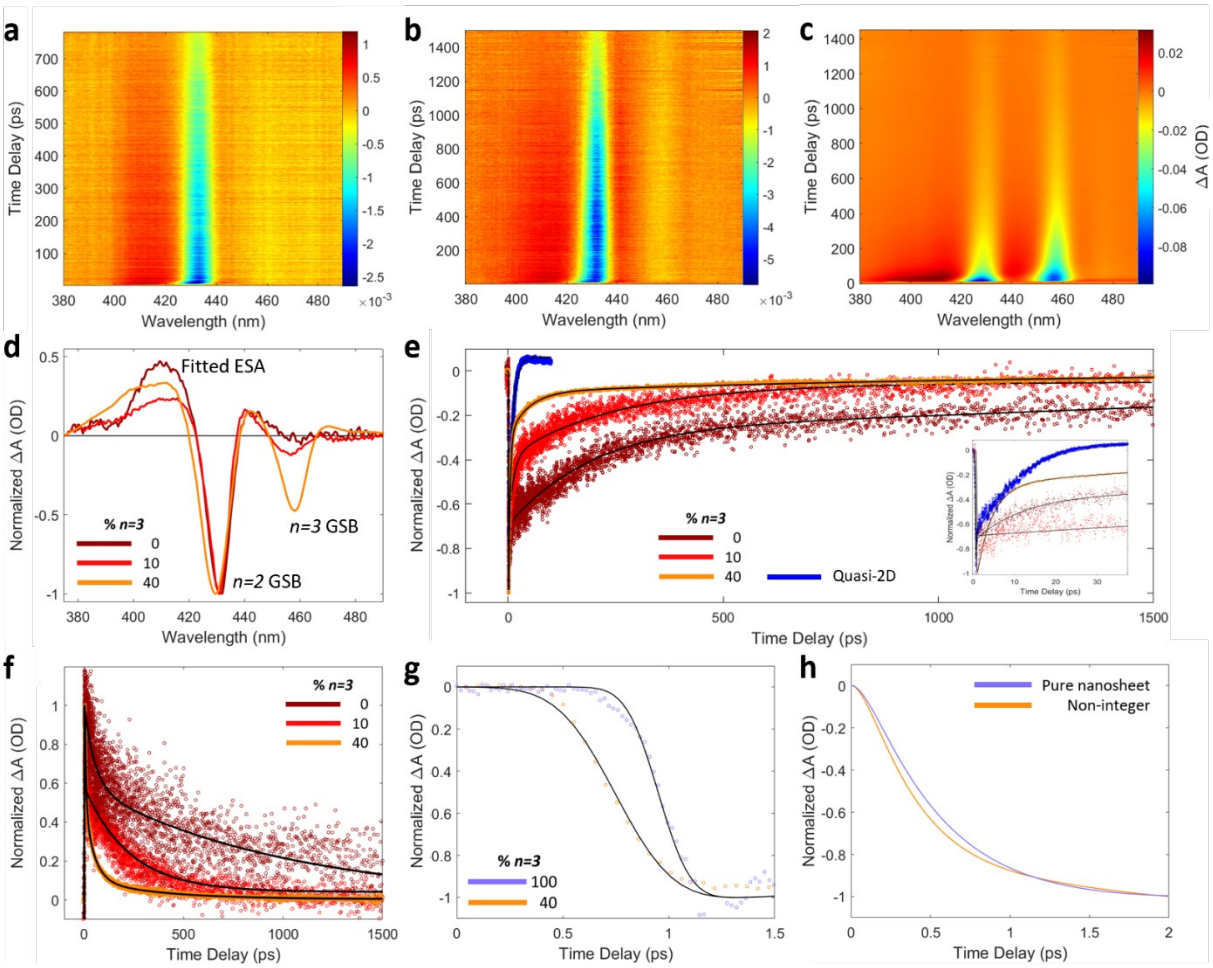

Figure 3. Photophysics of *n=2:3* $CsPbBr_3$ based on fsTA spectroscopy. 2D fsTA spectra of **a**, *n=2* $CsPbBr_3$ nanosheets, **b**, *n=2:3* $CsPbBr_3$ with 10% *n=3* composition, **c**, *n=2:3* $CsPbBr_3$ with 40% *n=3* composition. **d**, Spectral traces taken from **a-c** around a time delay of 1.5 ps. **e**, Quenching of the *n=2* GSB with increasing *n=3* composition, and compared with a quasi-2D perovskite. Inset: zoomed in view. **f**, Quenching of *n=2* GSB. **g**, The rise of the *n=3* GSB at 454 nm in the 40% *n=3* $CsPbBr_3$ compared to that of pure *n=3* nanosheet normalized to the fit. **h**, The modeled rise of the *n=3* GSB in the *n=3* nanosheet (without transfer) and in the *n=2:3* system (with transfer).

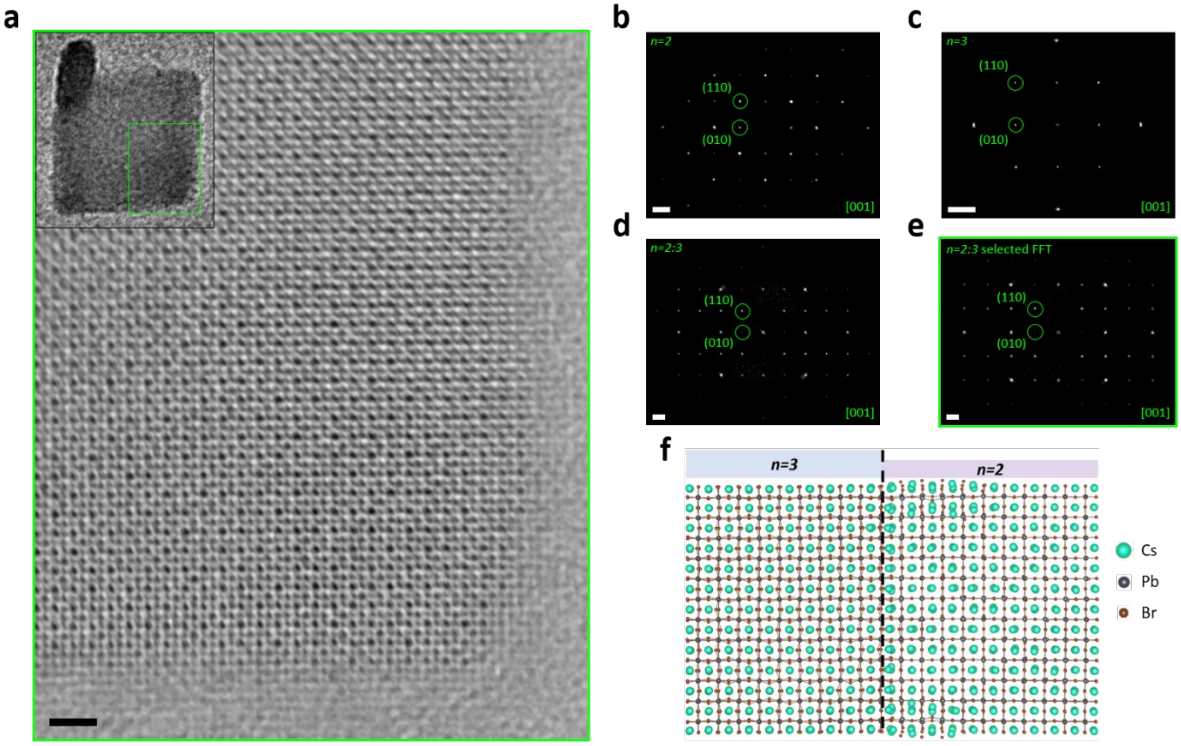

Figure 4. Atomic resolution characterization of *n=2:3* $CsPbBr_3$ interface. **a**, Aberration-corrected high resolution TEM image of non-integer $CsPbBr_3$ based on exit wave reconstruction. Scale bar: 2 nm. Inset: high-contrast image depicting the area of focus. FFT pattern, **b,** of the *n=2* nanosheet, **c**, *n=3* nanosheet, **d**, full *n=2:3* $CsPbBr_3$, and **e**, selected diffraction pattern around the *n=2:3* interface. Scale bar: 2 nm^{-1}. **f**, structural calculation of *n=2:3* $CsPbBr_3$.

ASSOCIATED CONTENT

Supporting Information.

Information about the methods, additional discussion on graphene encapsulation and the structural transformation reaction, characterization of n=2 and n=3 CsPbBr3 nanosheets, detailed steady-state and time-resolved optical spectroscopy data of all non-integer structures, computational results, raw atomic-resolution TEM data.

AUTHOR INFORMATION

Corresponding Author

Peidong Yang – Department of Chemistry, University of California, Berkeley, Berkeley, California 94720, United States; Department of Materials Science and Engineering, University of California, Berkeley, Berkeley, California 94720, United States; Materials Sciences Division, Lawrence Berkeley National Laboratory, Berkeley, California 94720, United States; 4 Kavli Energy NanoScience Institute, Berkeley, California 94720, United States; Email: p_yang@berkeley.edu

Authors

Alexander M. Oddo – Department of Chemistry, University of California, Berkeley, Berkeley, California 94720, United States; Materials Sciences Division, Lawrence Berkeley National Laboratory, Berkeley, California 94720, United States

Mengyu Gao – Department of Materials Science and Engineering, University of California, Berkeley, Berkeley, California 94720, United States**;** Materials Sciences Division, Lawrence Berkeley National Laboratory, Berkeley, California 94720, United States

Daniel Weinberg – Department of Chemistry, University of California, Berkeley, Berkeley, California 94720, United States**;** Materials Sciences Division, Lawrence Berkeley National Laboratory, Berkeley, California 94720, United States

Jianbo Jin – Department of Chemistry, University of California, Berkeley, Berkeley, California 94720, United States

Maria C. Folgueras – Department of Materials Science and Engineering, University of California, Berkeley, Berkeley, California 94720, United States**;** Materials Sciences Division, Lawrence Berkeley National Laboratory, Berkeley, California 94720, United States**;** Kavli Energy NanoScience Institute, Berkeley, California 94720, United States

Chengyu Song – National Center for Electron Microscopy, Molecular Foundry, Lawrence Berkeley National Laboratory, Berkeley, California 94720, United States

Colin Ophus – National Center for Electron Microscopy, Molecular Foundry, Lawrence Berkeley National Laboratory, Berkeley, California 94720, United States

Tomoyasu Mani – Department of Chemistry, University of Connecticut, Storrs, Connecticut 06269-3060, United States

Eran Rabani – Department of Chemistry, University of California, Berkeley, Berkeley, California 94720, United States**;** Materials Sciences Division, Lawrence Berkeley National

Laboratory, Berkeley, California 94720, United States; The Raymond and Beverly Sackler Center of Computational Molecular and Materials Science, Tel Aviv University, Tel Aviv 69978, Israel

Author Contributions

A.M.O., M.G., and P. Y. conceived the idea and designed the research. A.M.O. and M.G. led the study and contributed equally. D. W. performed the kinetic modeling and electronic structural calculations. D. W. and E. R. provided theoretical insight into the work. C. S. supervised and trained A.M.O. on the TEAM 0.5 microscope and C. O. provided the scripts for processing images taken on the TEAM 0.5 microscope. J.J. and M.C.F. contributed intellectually through numerous discussions. T.M. trained A.M.O. on fsTA spectroscopy. P.Y. supervised the work. All authors contributed to writing the manuscript.

Notes

The authors declare no competing interests.

ACKNOWLEDGMENT

The authors thank the staff at the NCEM, C. Song, C. Ophus, K. Bustillo, P. Ercius, and J. Ciston for their efforts in training the authors, A.M.O. and M.G., to use the electron microscopes. This work was supported by the U.S. Department of Energy, Office of Science, Office of Basic Energy Sciences, Materials Sciences and Engineering Division, under Contract No. DE-AC02–05-CH11231 within the Fundamentals of Semiconductor Nanowire Program (KCPY23). J.J acknowledges fellowship support from Suzhou Industrial Park. M.C.F acknowledges fellowship support from the Kavli ENSI Philomathia Graduate Student Fellowship.

REFERENCES

(1) Dey, A.; Ye, J.; De, A.; Debroye, E.; Ha, S. K.; Bladt, E.; Kshirsagar, A. S.; Wang, Z.; Yin, J.; Wang, Y.; et al. State of the Art and Prospects for Halide Perovskite Nanocrystals. *ACS Nano* **2021**, *15*, 10775–10981.

(2) Chen, Y.; Sun, Y.; Peng, J.; Tang, J.; Zheng, K.; Liang, Z. 2D Ruddlesden–Popper Perovskites for Optoelectronics. *Adv. Mater.* **2018**, *30*, 1703487.

(3) Gao, M.; Liu, H.; Yu, S.; Louisia, S.; Zhang, Y.; Nenon, D. P.; Alivisatos, A. P.; Yang, P. Scaling Laws of Exciton Recombination Kinetics in Low Dimensional Halide Perovskite Nanostructures. *J. Am. Chem. Soc.* **2020**, *142*, 8871–8879.

(4) Koscher, B. A.; Swabeck, J. K.; Bronstein, N. D.; Alivisatos, A. P. Essentially Trap-Free CsPbBr3 Colloidal Nanocrystals by Postsynthetic Thiocyanate Surface Treatment. *J. Am. Chem. Soc.* **2017**, *139*, 6566–6569.

(5) National Renewable Energy Laboratory. *Best research-cell efficiency chart.* National Renewable Energy Laboratory, 2023. https://www.nrel.gov/pv/assets/pdfs/best-research-cell-efficiencies.pdf (accessed 2023-10-17).

(6) Lee, K. J.; Wei, R.; Wang, Y.; Zhang, J.; Kong, W.; Chamoli, S. K.; Huang, T.; Yu, W.; ElKabbash, M.; Guo, C. Gigantic Suppression of Recombination Rate in 3D Lead-Halide Perovskites for Enhanced Photodetector Performance. *Nat. Photonics* **2023**, *17*, 236–243.

(7) Snaith, H. J. Present Status and Future Prospects of Perovskite Photovoltaics. *Nat. Mater.* **2018**, *17*, 372–376.

(8) Rong, Y.; Hu, Y.; Mei, A.; Tan, H.; Saidaminov, M. I.; Seok, S. Il; McGehee, M. D.; Sargent, E. H.; Han, H. Challenges for Commercializing Perovskite Solar Cells. *Science (80-.).* **2018**, *361*, eaat8235.

(9) Lee, J.-W.; Dai, Z.; Han, T.-H.; Choi, C.; Chang, S.-Y.; Lee, S.-J.; De Marco, N.; Zhao, H.; Sun, P.; Huang, Y.; et al. 2D Perovskite Stabilized Phase-Pure Formamidinium Perovskite Solar Cells. *Nat. Commun.* **2018**, *9*, 3021.

(10) Quan, L. N.; Yuan, M.; Comin, R.; Voznyy, O.; Beauregard, E. M.; Hoogland, S.; Buin, A.; Kirmani, A. R.; Zhao, K.; Amassian, A.; et al. Ligand-Stabilized Reduced-Dimensionality Perovskites. *J. Am. Chem. Soc.* **2016**, *138* (8), 2649–2655.

(11) Yuan, M.; Quan, L. N.; Comin, R.; Walters, G.; Sabatini, R.; Voznyy, O.; Hoogland, S.; Zhao, Y.; Beauregard, E. M.; Kanjanaboos, P.; et al. Perovskite Energy Funnels for Efficient Light-Emitting Diodes. *Nat. Nanotechnol.* **2016**, *11*, 872–877.

(12) He, T.; Li, S.; Jiang, Y.; Qin, C.; Cui, M.; Qiao, L.; Xu, H.; Yang, J.; Long, R.; Wang, H.; et al. Reduced-Dimensional Perovskite Photovoltaics with Homogeneous Energy Landscape. *Nat. Commun.* **2020**, *11*, 1672.

(13) Liu, J.; Leng, J.; Wu, K.; Zhang, J.; Jin, S. Observation of Internal Photoinduced Electron and Hole Separation in Hybrid Two-Dimentional Perovskite Films. *J. Am. Chem. Soc.* **2017**, *139* (4), 1432–1435.

(14) Lei, L.; Seyitliyev, D.; Stuard, S.; Mendes, J.; Dong, Q.; Fu, X.; Chen, Y.-A.; He, S.; Yi, X.; Zhu, L.; et al. Efficient Energy Funneling in Quasi-2D Perovskites: From Light Emission to Lasing. *Adv. Mater.* **2020**, *32*, 1906571.

(15) Zhou, N.; Shen, Y.; Li, L.; Tan, S.; Liu, N.; Zheng, G.; Chen, Q.; Zhou, H. Exploration of Crystallization Kinetics in Quasi Two-Dimensional Perovskite and High Performance Solar Cells. *J. Am. Chem. Soc.* **2018**, *140*, 459–465.

(16) Zhang, D.; Fu, Y.; Liu, C.; Zhao, C.; Gao, X.; Zhang, J.; Guo, W.; Liu, J.; Qin, C.; Wang, L. Domain Controlling by Compound Additive toward Highly Efficient Quasi-2D Perovskite Light-Emitting Diodes. *Adv. Funct. Mater.* **2021**, *31*, 2103890.

(17) Wang, T.; Dong, Y.; Guo, J.; Li, Q.; Chang, Z.; Chen, M.; Wang, R.; Liu, Y. Integrated Quasi-2D Perovskite/Organic Solar Cells with Efficiency over 19% Promoted by Interface Passivation. *Adv. Funct. Mater.* **2021**, *31*, 2107129.

(18) Wang, Z.; Wei, Q.; Liu, X.; Liu, L.; Tang, X.; Guo, J.; Ren, S.; Xing, G.; Zhao, D.; Zheng, Y. Spacer Cation Tuning Enables Vertically Oriented and Graded Quasi-2D Perovskites for Efficient Solar Cells. *Adv. Funct. Mater.* **2021**, *31*, 2008404.

(19) Quan, L. N.; Zhao, Y.; García de Arquer, F. P.; Sabatini, R.; Walters, G.; Voznyy, O.; Comin, R.; Li, Y.; Fan, J. Z.; Tan, H.; et al. Tailoring the Energy Landscape in Quasi-2D Halide Perovskites Enables Efficient Green-Light Emission. *Nano Lett.* **2017**, *17* (6), 3701–3709.

(20) Yin, J.; Brédas, J.-L.; Bakr, O. M.; Mohammed, O. F. Boosting Self-Trapped Emissions in Zero-Dimensional Perovskite Heterostructures. *Chem. Mater.* **2020**, *32*, 5036–5043.

(21) Sun, Y.; Dai, S. High-Entropy Materials for Catalysis: A New Frontier. *Sci. Adv.* **2022**, *7*, eabg1600.

(22) Parobek, D.; Roman, B. J.; Dong, Y.; Jin, H.; Lee, E.; Sheldon, M.; Son, D. H. Exciton-to-Dopant Energy Transfer in Mn-Doped Cesium Lead Halide Perovskite Nanocrystals. *Nano Lett.* **2016**, *16*, 7376–7380.

(23) Leveillee, J.; Katan, C.; Even, J.; Ghosh, D.; Nie, W.; Mohite, A. D.; Tretiak, S.; Schleife, A.; Neukirch, A. J. Tuning Electronic Structure in Layered Hybrid Perovskites with Organic Spacer Substitution. *Nano Lett.* **2019**, *19*, 8732–8740.

(24) Calvin, J. J.; Brewer, A. S.; Alivisatos, A. P. The Role of Organic Ligand Shell Structures in Colloidal Nanocrystal Synthesis. *Nat. Synth.* **2022**, *1*, 127–137.

(25) Lei, Y.; Li, Y.; Lu, C.; Yan, Q.; Wu, Y.; Babbe, F.; Gong, H.; Zhang, S.; Zhou, J.; Wang, R.; et al. Perovskite Superlattices with Efficient Carrier Dynamics. *Nature* **2022**, *608*, 317–323.

(26) Rainò, G.; Becker, M. A.; Bodnarchuk, M. I.; Mahrt, R. F.; Kovalenko, M. V; Stöferle, T. Superfluorescence from Lead Halide Perovskite Quantum Dot Superlattices. *Nature* **2018**, *563*, 671–675.

(27) Cherniukh, I.; Rainò, G.; Stöferle, T.; Burian, M.; Travesset, A.; Naumenko, D.; Amenitsch, H.; Erni, R.; Mahrt, R. F.; Bodnarchuk, M. I.; et al. Perovskite-Type Superlattices from Lead Halide Perovskite Nanocubes. *Nature* **2021**, *593*, 535–542.

(28) Liu, Y.; Siron, M.; Lu, D.; Yang, J.; dos Reis, R.; Cui, F.; Gao, M.; Lai, M.; Lin, J.; Kong, Q.; et al. Self-Assembly of Two-Dimensional Perovskite Nanosheet Building Blocks into Ordered Ruddlesden–Popper Perovskite Phase. *J. Am. Chem. Soc.* **2019**, *141* (33), 13028–13032.

(29) Zhang, Y.; Lu, D.; Gao, M.; Lai, M.; Lin, J.; Lei, T.; Lin, Z.; Quan, L. N.; Yang, P. Quantitative Imaging of Anion Exchange Kinetics in Halide Perovskites. *Proc. Natl. Acad. Sci.* **2019**, *116*, 12648–12653.

(30) Akriti; Shi, E.; Shiring, S. B.; Yang, J.; Atencio-Martinez, C. L.; Yuan, B.; Hu, X.; Gao, Y.; Finkenauer, B. P.; Pistone, A. J.; et al. Layer-by-Layer Anionic Diffusion in Two-Dimensional Halide Perovskite Vertical Heterostructures. *Nat. Nanotechnol.* **2021**, *16*, 584–591.

(31) Imran, M.; Peng, L.; Pianetti, A.; Pinchetti, V.; Ramade, J.; Zito, J.; Di Stasio, F.; Buha, J.; Toso, S.; Song, J.; et al. Halide Perovskite–Lead Chalcohalide Nanocrystal Heterostructures. *J. Am. Chem. Soc.* **2021**, *143*, 1435–1446.

(32) Xu, F.; Meng, K.; Cheng, B.; Wang, S.; Xu, J.; Yu, J. Unique S-Scheme Heterojunctions in Self-Assembled TiO2/CsPbBr3 Hybrids for CO2 Photoreduction. *Nat. Commun.* **2020**, *11*, 4613.

(33) Wang, Y.; Wu, T.; Barbaud, J.; Kong, W.; Cui, D.; Chen, H.; Yang, X.; Han, L. Stabilizing Heterostructures of Soft Perovskite Semiconductors. *Science (80-.).* **2019**, *365*, 687–691.

(34) Pedetti, S.; Ithurria, S.; Heuclin, H.; Patriarche, G.; Dubertret, B. Type-II CdSe/CdTe Core/Crown Semiconductor Nanoplatelets. *J. Am. Chem. Soc.* **2014**, *136*, 16430–16438.

(35) Tessier, M. D.; Spinicelli, P.; Dupont, D.; Patriarche, G.; Ithurria, S.; Dubertret, B. Efficient Exciton Concentrators Built from Colloidal Core/Crown CdSe/CdS Semiconductor Nanoplatelets. *Nano Lett.* **2014**, *14*, 207–213.

(36) Yang, A. J.; Han, K.; Huang, K.; Ye, C.; Wen, W.; Zhu, R.; Zhu, R.; Xu, J.; Yu, T.; Gao, P.; et al. Van Der Waals Integration of High-κ Perovskite Oxides and Two-Dimensional Semiconductors. *Nat. Electron.* **2022**, *5*, 233–240.

(37) Leng, K.; Wang, L.; Shao, Y.; Abdelwahab, I.; Grinblat, G.; Verzhbitskiy, I.; Li, R.; Cai, Y.; Chi, X.; Fu, W.; et al. Electron Tunneling at the Molecularly Thin 2D Perovskite and Graphene van Der Waals Interface. *Nat. Commun.* **2020**, *11*, 5483.

(38) Wang, Q.; Zhang, Q.; Luo, X.; Wang, J.; Zhu, R.; Liang, Q.; Zhang, L.; Yong, J. Z.; Yu Wong, C. P.; Eda, G.; et al. Optoelectronic Properties of a van Der Waals WS2 Monolayer/2D Perovskite Vertical Heterostructure. *ACS Appl. Mater. Interfaces* **2020**, *12*, 45235–45242.

(39) Gao, P.; Bin Mohd Yusoff, A. R.; Nazeeruddin, M. K. Dimensionality Engineering of Hybrid Halide Perovskite Light Absorbers. *Nat. Commun.* **2018**, *9*, 5028.

(40) Teale, S.; Proppe, A. H.; Jung, E. H.; Johnston, A.; Parmar, D. H.; Chen, B.; Hou, Y.; Kelley, S. O.; Sargent, E. H. Dimensional Mixing Increases the Efficiency of 2D/3D Perovskite Solar Cells. *J. Phys. Chem. Lett.* **2020**, *11*, 5115–5119.

(41) Passarelli, J. V; Mauck, C. M.; Winslow, S. W.; Perkinson, C. F.; Bard, J. C.; Sai, H.; Williams, K. W.; Narayanan, A.; Fairfield, D. J.; Hendricks, M. P.; et al. Tunable Exciton Binding Energy in 2D Hybrid Layered Perovskites through Donor–Acceptor Interactions within the Organic Layer. *Nat. Chem.* **2020**, *12*, 672–682.

(42) Panuganti, S.; Besteiro, L. V; Vasileiadou, E. S.; Hoffman, J. M.; Govorov, A. O.; Gray, S. K.; Kanatzidis, M. G.; Schaller, R. D. Distance Dependence of Förster Resonance Energy Transfer Rates in 2D Perovskite Quantum Wells via Control of Organic Spacer Length. *J. Am. Chem. Soc.* **2021**, *143*, 4244–4252.

(43) Xi, J.; Spanopoulos, I.; Bang, K.; Xu, J.; Dong, H.; Yang, Y.; Malliakas, C. D.; Hoffman, J. M.; Kanatzidis, M. G.; Wu, Z. Alternative Organic Spacers for More Efficient Perovskite Solar Cells Containing Ruddlesden–Popper Phases. *J. Am. Chem. Soc.* **2020**, *142*, 19705–19714.

(44) Sun, J.-K.; Huang, S.; Liu, X.-Z.; Xu, Q.; Zhang, Q.-H.; Jiang, W.-J.; Xue, D.-J.; Xu, J.-C.; Ma, J.-Y.; Ding, J.; et al. Polar Solvent Induced Lattice Distortion of Cubic CsPbI3 Nanocubes and Hierarchical Self-Assembly into Orthorhombic Single-Crystalline Nanowires. *J. Am. Chem. Soc.* **2018**, *140*, 11705–11715.

(45) Bekenstein, Y.; Koscher, B. A.; Eaton, S. W.; Yang, P.; Alivisatos, A. P. Highly Luminescent Colloidal Nanoplates of Perovskite Cesium Lead Halide and Their Oriented Assemblies. *J. Am. Chem. Soc.* **2015**, *137*, 16008–16011.

(46) Yu, Y.; Zhang, D.; Kisielowski, C.; Dou, L.; Kornienko, N.; Bekenstein, Y.; Wong, A. B.; Alivisatos, A. P.; Yang, P. Atomic Resolution Imaging of Halide Perovskites. *Nano Lett.* **2016**, *16* (12), 7530–7535.

(47) Gao, M.; Park, Y.; Jin, J.; Chen, P.-C.; Devyldere, H.; Yang, Y.; Song, C.; Lin, Z.; Zhao, Q.; Siron, M.; et al. Direct Observation of Transient Structural Dynamics of Atomically Thin Halide Perovskite Nanowires. *J. Am. Chem. Soc.* **2023**, *145*, 4800–4807.

(48) Proppe, A. H.; Elkins, M. H.; Voznyy, O.; Pensack, R. D.; Zapata, F.; Besteiro, L. V; Quan, L. N.; Quintero-Bermudez, R.; Todorovic, P.; Kelley, S. O.; et al. Spectrally Resolved Ultrafast Exciton Transfer in Mixed Perovskite Quantum Wells. *J. Phys. Chem. Lett.* **2019**, *10*, 419–426.

(49) Gan, Z.; Chen, W.; Zhou, C.; Yu, L.; Dong, L.; Jia, B.; Wen, X. Efficient Energy Funnelling by Engineering the Bandgap of a Perovskite: Förster Resonance Energy Transfer or Charge Transfer? *J. Phys. Chem. Lett.* **2020**, *11*, 5963–5971.

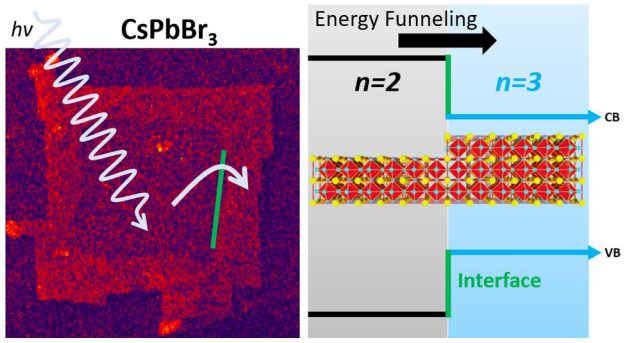

For Table of Contents use only.